Parity nonconservation in proton-nucleus scattering at 6 GeV/c

N. Lockyer* and T. A. Romanowski
Department of Physics, Ohio State University, Columbus, Ohio 43210

J. D. Bowman, C. M. Hoffman, R. E. Mischke, D. E. Nagle, J. M. Potter, and R. L. Talaga†
University of California, Los Alamos National Laboratory, Los Alamos, New Mexico 87545

E. C. Swallow‡
Department of Physics, Elmhurst College, Elmhurst, Illinois 60126
and Enrico Fermi Institute, University of Chicago, Chicago, Illinois 60637

D. M. Alde§
Department of Physics, University of Illinois, Urbana, Illinois 61801

D. R. Moffett**
Argonne National Laboratory, Argonne, Illinois 60439

J. Zyskind††
Department of Physics and Astronomy, California Institute of Technology, Pasadena, California 91109
(Received 21 February 1984)

A parity-nonconserving asymmetry in the total cross section for 6-GeV/c polarized protons on a water target has been measured. The experiment used two independent detector systems to measure the helicity dependence of the transmission through the target. Special attention was paid to possible sources of systematic errors. The result is $A_L=(2.65\pm0.60\pm0.36)\times10^{-6}$ where $A_L=(\sigma_+-\sigma_-)/(\sigma_++\sigma_-)$ is the fractional difference of the total cross sections for positive- and negative-helicity protons on an unpolarized target. The first error is statistical and the second is an estimate of systematic uncertainties. This result is much larger than predictions based on meson-exchange calculations but consistent with a recent QCD calculation.

I. INTRODUCTION

This paper describes the last in a series of experiments[1–5] to search for parity nonconservation in proton-nucleus scattering using the 6-GeV/c polarized proton beam at the Argonne National Laboratory Zero Gradient Synchrotron (ZGS). The experiment measured the helicity dependence of the total cross section for the scattering of polarized protons from a water target. The result for the longitudinal asymmetry A_L is

$$A_L=\frac{\sigma_+-\sigma_-}{\sigma_++\sigma_-}=(2.65\pm0.60\pm0.36)\times10^{-6}\,, \qquad (1)$$

where σ_+ (σ_-) is the total scattering cross section for the interaction of protons in a positive- (negative-) helicity state. The first error is statistical and the second is an estimate of systematic uncertainties.

A helicity dependence is expected from an interference between weak and strong scattering amplitudes. Measurements of A_L for proton-proton scattering at low energies have yielded a value[6] of $(-1.7\pm0.8)\times10^{-7}$ at 15 MeV and a result[7,8] of $(-2.3\pm0.8)\times10^{-7}$ at 45 MeV, in agreement with calculations.[9–14]

The first measurement at 6 GeV/c gave the result $A_L=(5\pm9)\times10^{-6}$ using a beryllium target.[1] A value $A_L=(-15.0\pm2.8)\times10^{-6}$ was obtained when the experiment was repeated using a water target.[2] At that time, it was realized that a nonzero transmission asymmetry can result from the production and subsequent decay of longitudinally polarized hyperons. Consequently, the next version of the experiment was designed with a focusing magnetic spectrometer to eliminate hyperon-decay products.[3]

The value of A_L found in the present experiment[5] for water is an order of magnitude larger than the theoretical predictions[15,16] for pp and pn scattering that predated our measurement. The large discrepancy has stimulated several additional theoretical studies. Further discussion of the theoretical predictions is given in Sec. V. The experimental method and apparatus used in the experiment are described in Sec. II and the data collection in Sec. III. Section IV describes the analysis and is followed by the results and discussion in Sec. V.

II. EXPERIMENTAL METHOD

A. General approach

In this section an outline of the experimental method is given; the details of the apparatus are presented later. The experiment determined total cross sections by measuring the transmission Z through a water target. Two independent detector systems measured the number of protons upstream and downstream of the target for

each beam pulse. The detector currents were integrated, as the required beam intensities prohibited counting individual protons. The first detector system used scintillation counters. For this system, the transmission for one pulse of protons from the ZGS was measured as

$$Z_1 = T/I \ , \tag{2}$$

where T and I are the signals from the downstream and upstream counters, respectively. (The notation for signals corresponds to the detectors from which they are derived.) The second system used three identical ionization chambers. For each pulse, the signal from the downstream chamber D was subtracted from the signal of the upstream chamber U and normalized to that from the monitor chamber M (located upstream). Thus we took

$$1 - Z_2 = (U - D)/M \ . \tag{3}$$

By adjusting the pressure in chamber D to cancel the signal from chamber U, a null balance was obtained.

Because each successive beam pulse had opposite helicity, the fractional change in transmission for each pair of pulses is (dropping the indices 1 and 2 that designate the detector systems)

$$\frac{\Delta Z}{2Z} = \frac{Z_+ - Z_-}{Z_+ + Z_-} \ , \tag{4}$$

where Z_+ (Z_-) is the transmission (from either detector system) for the positive- (negative-) helicity pulse.

Fluctuations in ΔZ resulted from statistical uncertainties in the measurements of Z and from changes in Z due, for example, to random fluctuations in beam properties. The dependence of Z on beam motion and intensity fluctuations was removed by defining a corrected transmission Z', for each pulse given by

$$Z' = Z - a_1(x - x_0)^2 - a_2(y - y_0)^2 - a_3(\langle i^2 \rangle / I) \ . \tag{5}$$

Here $(x - x_0)$ and $(y - y_0)$ are horizontal and vertical deviations of the beam from the symmetry axis of the experiment (given by x_0, y_0). A measure of the time structure of the beam within a beam pulse is given by the square of the instantaneous beam intensity, $\langle i^2 \rangle$, normalized to the beam intensity for the whole pulse, I. The dependence of Z on position is quadratic in lowest order because the beam was centered on a collimator and a displacement in any direction caused Z to decrease. The coefficients a_i were determined from a linear-regression analysis to minimize fluctuations in Z'.

An average $\langle \Delta Z'/2Z' \rangle$ was calculated for each run. The uncertainty in $\langle \Delta Z'/2Z' \rangle$ was determined from rms fluctuations in $\Delta Z'/2Z'$ and is designated $\delta\langle \Delta Z'/2Z' \rangle$. Corrections were applied to the $\langle \Delta Z'/2Z' \rangle$ from each run for known background processes that could give a change of transmission correlated with helicity, yielding

$$\langle \Delta Z'/2Z' \rangle' = \langle \Delta Z'/2Z' \rangle - \sum_i \gamma_i d_i \langle \Delta H_i' \rangle \ , \tag{6}$$

where γ (cm^{-1}) is the sensitivity constant for the term, d (cm) is the displacement of the beam from the symmetry axis, and $\langle \Delta H \rangle$ is the average change of a polarization-correlated quantity. The values of the H and d quantities were monitored each beam pulse and the γ values were measured in calibration runs.

Consider, for example, the effect of a residual transverse polarization of the beam, which leads to a parity-allowed left-right or up-down scattering asymmetry. The residual transverse polarization changes sign as the beam helicity is reversed and, if the beam is not centered on the collimator, a change occurs in the measured transmission. The sensitivity of the transmission to transverse polarization as a function of the beam displacement from the symmetry axis was measured in calibration runs where horizontal or vertical components of polarization were introduced using solenoids in the beam line.

Another source of asymmetry was beam scattered by the small amount of material in those parts of the beam channel where the polarization was fully vertical. The scattered beam produced a signal in the I counter and U chamber that was correlated with beam helicity (to the extent that the beam was displaced from the effective center of the upstream detectors). In the runs measuring this so-called beam-matter interaction, the interaction probability was increased by adding a known amount of material in the channel and measuring the asymmetry.

After all runs were combined, a correction for the correlation between transverse polarization and position within the beam was applied to the weighted average. This last correction is given by $\gamma\epsilon$ where γ is the sensitivity to transverse polarization mentioned above and ϵ is the spatial first moment of the beam-polarization distribution:

$$\epsilon = \int\int dx\, dy [x R_y(x,y) - y R_x(x,y)] B(x,y) \ . \tag{7}$$

x and y are particle coordinates at the collimator, $R_x(x,y)$ and $R_y(x,y)$ are the transverse polarization components for a given beam helicity, and $B(x,y)$ represents the intensity distribution of the beam. It can be seen that a transverse component of polarization that averages to zero can produce a spurious parity signal.

To determine ϵ, the average helicity-correlated components of polarization, $\langle \Delta R_y \rangle$ ($\langle \Delta R_x \rangle$) were measured for the left and right (upper and lower) halves of the beam separately by blocking off half the beam for each measurement. We define

$$\langle \Delta R_x \rangle = \langle R_x \rangle_+ - \langle R_x \rangle_- \ , \tag{8}$$

where $\langle R_x \rangle_\pm$ is defined by an integral over half the beam for a pulse with $\pm$ helicity:

$$\langle R_x \rangle = \frac{\int\int dx\, dy\, R_x B(x,y)}{\int\int dx\, dy\, B(x,y)} \ . \tag{9}$$

A similar expression applies for $\langle \Delta R_y \rangle$. Thus Eq. (7) can be written as

$$\epsilon = a(\langle \Delta R_x \rangle - \langle \Delta R_y \rangle) \ , \tag{10}$$

where the coefficient a depends on the beam shape and the distribution of polarization across the beam. The polarization distribution arises from the process of extraction from the ZGS and from the effect of fringe fields in the magnetic transport of the beam. The known air and solid matter in the beam line broaden the beam size by

about a factor of two due to multiple scattering. One consequence is that the beam profile is Gaussian. Second, any higher-order components of the polarization distribution are washed out. As a result, a linear variation of polarization with position is expected with a Gaussian beam-intensity shape, yielding $a=-\sqrt{2\pi}/8$. The value of a changes by 10% for extreme alternate assumptions about the beam and initial polarization distributions.

Each of the steps outlined in this section are discussed quantitatively in the analysis section. After all corrections have been applied, the value of $\langle \Delta Z'/2Z' \rangle$ is converted to the corresponding value of A_L.

B. Hyperon-decay products

The incident-proton-beam helicity may be transferred to decay products of hyperons produced in the target resulting in a helicity dependent transmission asymmetry. For example, in the decay $\Lambda^0 \rightarrow p\pi^-$, the protons emerge preferentially along the direction of the Λ polarization and the pions preferentially against. Because the proton carries most of the Λ longitudinal momentum, it will have an angular distribution peaked more forward in the laboratory frame than the pion (± 60 mr for the protons compared to ± 200 mr for the pions). As the beam helicity is reversed, the angular distribution of the decay products is modified; the effect is largest for the pions. This gives rise to a helicity-correlated signal. A collimator was inserted 1.58 m downstream of the center of the target that transmitted only 10% of the protons and 1% of the pions from Λ decay and less than 0.5% of the Λ's. In addition, a focusing magnetic spectrometer was installed to transmit only particles with the beam momentum minus the momentum loss in the target. This eliminated the decay products of the polarized hyperons produced in the target and therefore removed the spurious parity signal that could be caused by hyperon-decay products striking the transmission detectors.

C. Apparatus

1. Polarized proton beam

The 6-GeV/c beam from the ZGS had an average polarization $\langle \vec{P} \rangle = 0.71 \pm 0.03$, an average intensity of 3.2×10^8 protons/pulse, a spill width of roughly 700 ms, and a repetition rate of 0.3 Hz. The polarization direction was reversed at the source each ZGS pulse. The polarization was vertical during acceleration in the synchrotron and remained so in the external proton beam.

A plan view of the beam line and apparatus is shown in Fig. 1. Most of the beam line was evacuated but the beam encountered the vacuum windows and air in some regions. The septum magnet SB1 separated our beam from the external proton beam. The bending magnets SB2 and $B1$ controlled horizontal position and angle of the beam through our apparatus. The magnet $B2$ deflected the beam upward through 7.75° to rotate the transverse polarization into the longitudinal direction. A proton with polarization up (down) rotated into a negative- (positive-) helicity state.

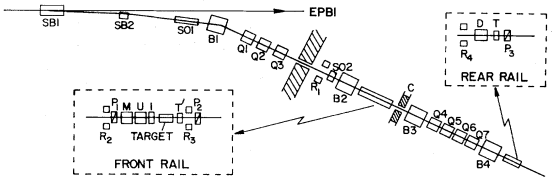

FIG. 1. Schematic diagram of the beam line and apparatus. Detectors and beam-line components are described in the text.

Solenoids in the beam line were used to control the transverse polarization of the beam at the target. The solenoid triplet SO1 rotated the spin (by as much as 3.6°) from vertical in a plane normal to the beam direction. This horizontal spin component rotated almost completely into the longitudinal direction during a 6° bend of the beam by magnet $B1$ and became a vertical component after $B2$. The solenoid SO2 was located after the horizontal bend in the beam line and was used to control the horizontal component of the beam polarization.

The quadrupole triplet $Q1$, $Q2$, and $Q3$ focused the beam on the 5.5-cm-diameter aperture of a 46.3-cm-long brass collimator C, located after the target. The spot size at C was 2.3 cm horizontal and 2.6 cm vertical (full width at half maximum). The spectrometer consisted of two bending magnets and four quadrupole magnets. Each bending magnet ($B3$ and $B4$) bent the beam downward and rotated the spin direction by 90° in the vertical plane. The inner diameter of the evacuated channel between $B3$ and $B4$, where the proton spin was transverse, was 22.9 cm. Quadrupoles $Q4$—$Q7$ focused the beam onto the transmission detectors to a spot size of 2.0 cm in diameter. The momentum dispersion of the spectrometer was 1.1 cm/(% $\Delta p/p$).

2. Water target

The target was distilled water, enclosed in an aluminum cylindrical container, 81 cm long and 15.2 cm in diameter. The container windows were made of 0.32-cm-thick flat quartz glass and were aligned parallel to each other and perpendicular to the incident-beam direction. This design ensured that each beam particle encountered the same amount of material in the target. The transmission coefficient of the target was $Z = 0.18 \pm 0.01$.

3. Detector systems

Most of the detectors were mounted on two rigid rails. (See Fig. 1 and the relative positions given in Table I.) The magnets and experimental apparatus were aligned by optical survey. In addition to the scintillation counters and ionization chambers for the transmission measurement, auxiliary scintillation counters measured various properties of the polarized proton beam. The alignment of the auxiliary detectors was not critical because signals from the detectors were balanced in the electronics.

(a) Scintillation counters. Three scintillation counters were used for the transmission measurement. Each of these counters had a block of scintillator, $10 \times 10 \times 2.5$

TABLE I. Positions of apparatus. The SPIC and SIC devices were beam-position and intensity detectors provided by the ZGS.

Device	Length (m)	Distance from entrance to cave (m)
SIC		0
R_1		0.11
SPIC		0.22
SO2	0.70	0.82
$B2$	2.40	2.37
R_2		4.06
P_1		4.26
M		4.50
U		4.80
I		5.00
Target	0.81	5.64
T'		6.81
R_3		6.93
P_2		7.03
SPIC		7.11
Collimator	0.46	7.44
Spectrometer	11.50	13.52
R_4		20.60
SPIC		20.70
D		20.90
T		21.20
P_3		21.75
SPIC		22.05
SIC		22.15

cm. The scintillator was connected to four Lucite light guides, $15\times10\times2.5$ cm, each followed by a 5-cm-long$\times$5-cm-diameter cylindrical light guide and a photomultiplier tube (PMT). The symmetrical arrangement of the PMT's about the beam direction helped to minimize the dependence of the summed signals on beam position. A fiber-optic cable, attached to each light guide, was used to inject a light pulse between each beam pulse for gain monitoring purposes. Counter I was located upstream of the target, T' was just downstream of the target, and T was placed after the spectrometer.

(b) Ionization chambers. Three ionization chambers were used. Each had a cylindrical active volume 20 cm long and 10 cm in diameter (see Fig. 2). Each collector plate had guard rings on either side spaced 0.75 mm away. A chamber had 20 collector plates and 21 high-voltage plates spaced 5 mm apart. Each plate was 25 μm thick in the active region. The entrance and exit windows were 1 mm thick and 10 cm in diameter. The active volume was defined by the guard rings and by the two outermost high-voltage plates.

Chambers U and D were operated in a null balance. The collector plates of U were connected to those of D by a low-capacitance coaxial cable. The high voltages applied to U and D were opposite in sign; the net current was nulled by adjusting the gas pressure in D. The third ion chamber M, measured the beam intensity and was used to normalize the difference signal. A gas mixture of 90% argon and 10% methane was used in all three chambers. The operating pressures were $\sim$40 psia for the M and D chambers and $\sim$8 psia for U.

(c) Auxiliary detectors. The beam position and polarization were measured every beam pulse by several sets of scintillation counters. Their positions are shown in Fig. 1 and their descriptions are given below.

The horizontal and vertical beam positions were measured by three sets of detectors with wedge-shaped scintillators P_1, P_2, and P_3. Two complementary wedges, forming a block of scintillator, $10\times10\times2.5$ cm, were optically isolated and connected to light guides and PMT's. Two such assemblies were mounted at right angles to each other and to the incident beam direction to form one position detector.

The R_1 and R_2 polarimeters measured the scattering

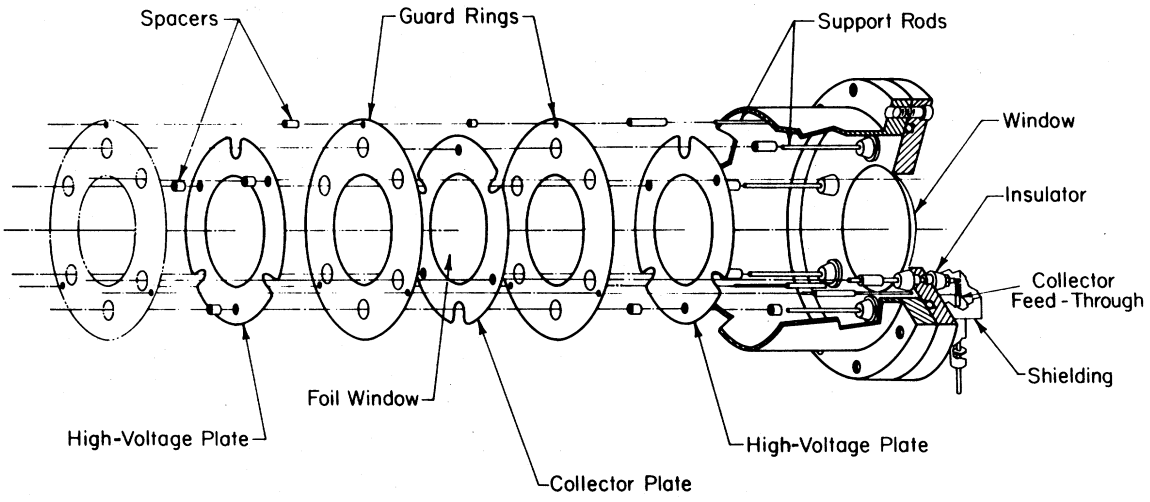

FIG. 2. Exploded view of a portion of an ionization-chamber assembly.

asymmetries at the entrance to the experimental area due to material in the beam line. The R_3 detector monitored residual transverse polarization by measuring the left-right and up-down scattering asymmetry of the beam scattered from the water target. The R_4 detector monitored scattering in the magnetic spectrometer. Each detector consisted of four plastic scintillator counters with active regions located to the left, right, above, and below the beam line. The R_1, R_2, and R_4 detectors consisted of four $10\times10\times2.5$-cm plastic scintillators with the centers 10 cm from beam center. The scintillators for R_3 were $7.5\times7.5\times2.5$-cm plastic scintillators with centers 11 cm from beam center.

4. *Time-structure monitor*

The instantaneous beam spill rate was monitored by squaring the voltage signal from the I detector with an analog circuit. The quantity formed is

$$\langle I^2\rangle = \int dt[i(t)]^2 , \tag{11}$$

where the integration is over the duration of the beam spill.

5. *Position feedback*

The beam centroid at position detector P_1 was stabilized pulse to pulse with the aid of a feedback loop. The voltage signals from the two horizontal PMT's of detector P_1 were used to control the current in magnet SB1. The time constant of the feedback loop, including the magnet response time, was ~100 ms.

6. *Signal processing*

Dumont 6292 PMT's were used for detectors P_1, P_2, P_3, I, T, R_3, and T'. They were selected to provide linear, noiseless gain with capability for a large dynamic range. For example, only five accelerating dynodes were used for the P_1, I, and T' detectors, which were exposed to the full intensity of the beam. Detectors R_1, R_2, and R_4 used ten-stage RCA 6342 PMT's. The current in each PMT was converted to a voltage by an operational amplifier and digitized by voltage-to-frequency converters (VTF's). The gain of each member of a group of detectors was matched to within 5%. The VTF output pulse train was scaled and recorded on magnetic tape each beam pulse.

The scintillator gating diagram is shown in Fig. 3(b). There were four intervals each cycle to record data. The duration of each interval was determined by a timing module that was triggered by a beam-start signal from the ZGS. There were two control signals: one gated the scalers and the other enabled or disabled the voltage signals at the VTF inputs via field-effect-transistor (FET) gates. The lengths of the scaler and FET gates were measured with a 20-MHz clock. The beam-associated data were recorded during the interval 1. For interval 2, the FET gate remained closed and the scalers were enabled allowing the electronic offsets to be measured. The PMT dark current was measured during interval 3. The relative gain of each phototube was measured during interval 4 using the fiber-optics system to insert a light pulse from a common source.

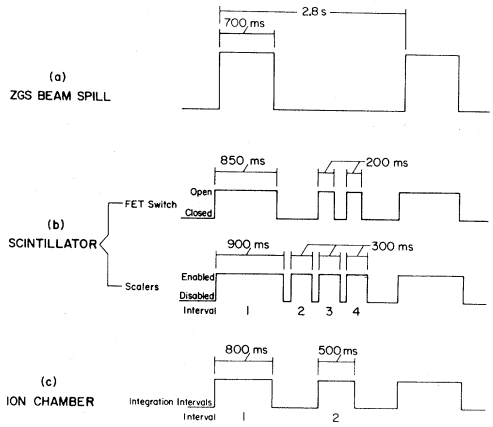

FIG. 3. Gated diagrams for the scintillator and ion-chamber signals. Beam-associated data were taken during interval 1, interval 2 was for electronic offset measurements, interval 3 was for dark-current measurements, and interval 4 was to check relative phototube gains.

For the ion-chamber system, the null current from U and D was amplified with a low-noise operational amplifier that converted the current to a voltage signal. The current from M was also amplified and converted to a voltage signal. These signals were digitized by VTF's and integrated in scalers. The amplifier gains and gas pressures were chosen such that the signals were about 1.0 V for each chamber.

The gating diagram for the ion-chamber system is shown in Fig. 3(c). There were two intervals each beam cycle to record data. The first interval was during the beam spill and extended in time to collect all charge. The second interval was used to measure electronic offsets, which were later subtracted from the counts from the first interval.

Data recorded each beam pulse included (a) integrated signal current from each phototube along with the electronic offset, dark current, and relative gain, (b) integrated signal currents from the ionization chamber system and electronic offsets, (c) analog and digital beam position and spot size from four ZGS proportional chambers, and beam intensity from two ZGS ionization chambers, (d) currents from ZGS extraction magnets, several beam-line magnets, and beam-polarization information from two ZGS polarimeters, and (e) two logic-level signals of opposite sense indicating the direction of polarization (up or down) of the incident proton beam.

III. EXPERIMENTAL PROCEDURE

A. Tuning and data acquisition

The beam-line magnet currents were adjusted to maximize the transmission of the beam through the apparatus using beam position and intensity monitors supplied by the ZGS. The beam was focused at the collimator, the smallest aperture in the beam line, to minimize the noise due to beam motion. A transmission quality factor Q was

defined as the ratio of measured fluctuations in the difference of transmission through the target for each helicity state to those fluctuations expected from statistical variations in the absorption process. The ratio for a run of N incident protons is

$$Q=\frac{\delta\langle \Delta Z/2Z\rangle}{[(1-Z)/ZN]^{1/2}} . \tag{12}$$

By systematically adjusting the beam magnet currents we could attain on-line Q factors between two and seven, for both detector systems. The off-line analysis could not remove these beam-induced transmission variations satisfactorily if the on-line Q factors were larger than about ten.

Finally, information from the calibration runs (Sec. IV B) allowed us to position the beam on the null or symmetry axis of the experiment where contributions from beam-matter effects were minimized.

There were 184 data runs with $\sim$1600 pulses/run for a total of $\sim 9\times 10^{13}$ protons on target. The rms variation of beam intensity was 4%. The rms resolution of the wedge detectors was about 15 μm. The pulse-to-pulse fluctuations of the beam position were 1 to 2 mm horizontally. In the vertical direction, beam motion was a factor of two smaller. Fast motion within a beam spill had amplitudes of up to $\sim$5 mm and these were unaffected by the slow feedback. The difference in the beam position between positive- and negative-helicity protons as measured by P_1, averaged over all the data, was 0.98 ± 0.68 μm in the horizontal direction and -0.70 ± 0.42 μm in the vertical direction.

The polarimeters monitored scattering asymmetries throughout the experiment and the results are incorporated into the correction terms in Eq. (6). The left-right scattering asymmetry measured with the R_3 detector was $(-4.7\pm 0.2)\times 10^{-5}$ and the up-down asymmetry was $(3.5\pm 0.5)\times 10^{-5}$ averaged over all data runs. With an analyzing power of -0.13, this gives a residual vertical polarization of $(3.62\pm 0.15)\times 10^{-4}$ and a horizontal polarization of $(-2.69\pm 0.40)\times 10^{-4}$ as compared to the longitudinal polarization of 0.71 ± 0.03 at the target. Beam scattering in the evacuated spectrometer channel was too small to be measured by the R_4 detector. The average left-right scattering asymmetry measured by the R_2 detector is $(3.500\pm 0.002)\times 10^{-3}$ due to material in the beam line.

B. Calibration

Three types of calibration runs were taken to measure the sensitivity coefficients γ, for the correction terms in Eq. (6). Each run consisted of $\sim$1600 pulses.

Eighteen residual-transverse-polarization runs were taken in two groups during the experiment. A horizontal or vertical polarization of $\sim$5% increased $\langle \Delta H\rangle=\langle \Delta R_{3x}\rangle$ or $\langle \Delta R_{3y}\rangle$ to $\sim 2.5\times 10^{-3}$. Data were recorded with $\langle \Delta R_{3y}\rangle$ nonzero at increments of a few mm in $\langle P_{2x}\rangle$ and similarly at intervals of $\langle P_{2y}\rangle$ for $\langle \Delta R_{3x}\rangle$ nonzero.

Added-absorber runs to measure the beam-matter interaction effects were taken with 5 cm of Lucite placed about 2 m upstream from the center of $B2$. Because the beam-matter interactions caused an asymmetric halo at the aperture of the I and U detectors that was monitored by the nearby R_2 detector, it was sufficient to enhance this asymmetry without reproducing the location and type of material. The Lucite caused an increase of $\langle \Delta R_{2y}\rangle$ by a factor of ten to $\sim 3.5\times 10^{-2}$. The beam was moved a few mm left and right of beam center while the absorber intercepted the entire incident beam. There were a total of 32 added-absorber runs, taken near the beginning and the end of the experiment. For these runs the magnet currents in $B2$ and the spectrometer were adjusted to transmit the lower energy beam caused by energy loss in the Lucite. Results are shown in Fig. 4. Additional data were taken with Lucite absorbers of 1 and 2 cm thickness. By extrapolating the asymmetry from the data with Lucite to zero added absorber, the amount of scattering taking place during nominal data runs were determined to be equivalent to 5 mm of Lucite absorber. This is consistent with the amount of material in the beam between SO1 and SO2 (300 cm of air, 0.53 cm of aluminum, and 0.03 cm of Mylar). Details of a Monte Carlo simulation of how the Lucite reproduced the effect of this material are given in Ref. 4.

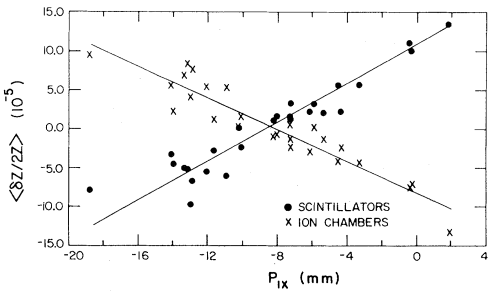

FIG. 4. Spurious parity signal versus beam position with 5 cm of Lucite intercepting the beam.

Beam-partially-blocked runs to measure the polarization distribution in the beam were taken with either the top, bottom, left, or right half of the beam removed with a collimator. A cylindrical brass collimator, 30 cm in length and 10.5 cm in diameter, filled the aperture at the downstream end of SO1. A combination of brass and styrofoam rods allowed the collimator to absorb one half of the beam while transmitting the other half. The results of the four runs are given in Table II.

TABLE II. Results of beam-partially-blocked runs.

Half of beam transmitted	R_y	R_x
Upper	$(2.75\pm 0.15)\times 10^{-4}$	$(0.60\pm 0.35)\times 10^{-4}$
Lower	-2.65 ± 0.20	1.60 ± 0.40
Right	0.50 ± 0.15	0.70 ± 0.15
Left	0.55 ± 0.20	1.45 ± 0.15

IV. ANALYSIS AND RESULTS

A. Introduction

The analysis had two main objectives: to produce a number representing the transmission asymmetry associated with helicity reversal, free from systematic contributions, and to minimize the uncertainty in this number.

The signal from each phototube for each pulse was obtained by subtracting electronic offsets and dark current as measured in the appropriate gating intervals. The algorithm involves, for variable X, the scaler counts from intervals 1 to 3 and the counts from the clock scaler, t, for the same intervals. The signal for scintillator X is

$$X=\left[\frac{X(s1)-X(s2)t(s1)/t(s2)}{t(f1)}\right]-\left[\frac{X(s3)-X(s2)t(s3)/t(s2)}{t(f2)}\right], \quad (13)$$

where s and f correspond to the scaler and FET times, respectively, and the numbers refer to the intervals defined in Fig. 3. A similar algorithm applies for the ion-chamber signals.

B. Data-selection procedure

The data-selection procedure eliminated data from beam pulses with poor beam quality. The procedure used "quads" for variables P_{1x}, $P_{1x}{}^2$, P_{1y}, M, Z_1, and Z_2. A quad for a measured variable X is defined as

$$X^q=X_i-X_{i+1}-X_{i+2}+X_{i+3}\ ,$$

where pulse i has positive helicity. A quad has zero net polarization, an average value, $\langle X^q\rangle$, of zero, and is not affected by a linear gain drift during the four pulses. Acceptable quads had all beam pulses with more than 5×10^7 incident protons and no variables with negative offsets. The distribution of values of X^q is generally Gaussian and centered at zero but has enhanced tails. Because of these tails, we define the width of the distribution as $\delta\langle X^q\rangle=0.69(X^m)$ where X^m is the median of the absolute values of the quads. If X^q was greater than 2.5 $\delta\langle X^q\rangle$ for any of the six variables listed above, the data from the four beam pulses were rejected. These criteria removed about 10% of the data from each run.

C. Linear-regression analysis

The pulse-to-pulse fluctuations in the measured transmission of the beam through the apparatus were caused by detector noise, statistical variations in the absorption of the beam in the target, and from temporal changes in beam properties. A regression analysis was employed to reduce the effects of beam properties on the measured transmission. An example of the dependence of the transmission on position, clearly exhibiting the quadratic dependence, is shown in Fig. 5.

Equation (5) can be rewritten in an expanded form as

$$Z'=Z-a_1(P_{1x}-P_{1x_0})^2-a_2(P_{1y}-P_{1y_0})^2-a_3(\langle i^2\rangle/I)\ , \quad (14)$$

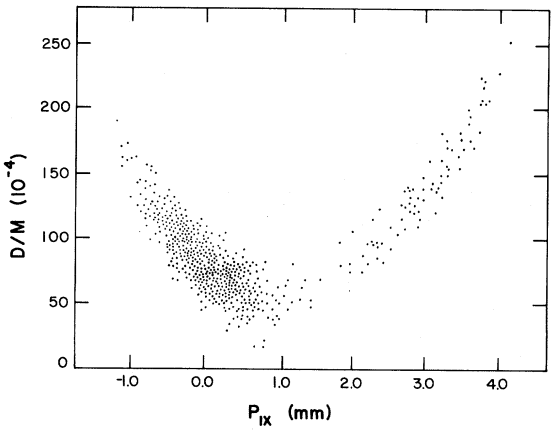

FIG. 5. Scatter plot of transmission versus horizontal position. These data illustrate the quadratic dependence and are not typical of normal data.

where x_0 (y_0) is the center of the collimator as measured by P_1. (Detector P_2 was closer to the collimator but P_1 was used because it had less noise.) The evaluation of the coefficients was based on an analysis using the quad values of the variables. This made the results insensitive to any correlation between beam helicity and position or intensity. The summary of contributions to $\langle\Delta Z'/2Z'\rangle$ averaged over all runs is given in Table III. Note that there is no evidence for a helicity correlation with these variables since each of the contributions is consistent with zero.

The data from the R_1, R_2, and R_3 polarimeters were treated in a similar manner to remove position sensitivity in the polarization values.

D. Beam-matter interaction and residual polarization

The next stage of the analysis corrected for known helicity-correlated quantities based on Eq. (6). The terms for residual transverse polarization, which mostly affected the T and D signals, can be written

$$\sum\gamma_i d_i\langle\Delta H_i'\rangle=\gamma_1(P_{2x}-P_{2x_0})\langle\Delta R'_{3y}\rangle+\gamma_2(P_{2y}-P_{2y_0})\langle\Delta R'_{3x}\rangle\ . \quad (15)$$

TABLE III. Summary of contributions to $\langle\Delta Z/2Z\rangle$ from beam properties.

Property	Scintillators	Ion chambers
Horizontal position	$(-0.09\pm0.46)\times10^{-6}$	$(-0.32\pm0.34)\times10^{-6}$
Vertical position	-0.22 ± 0.33	-0.12 ± 0.21
Time structure	$+0.04\pm0.03$	$+0.01\pm0.01$
Sum	-0.27 ± 0.57	-0.43 ± 0.40

TABLE IV. Contributions to $\langle \Delta Z'/2Z' \rangle$ from background processes.

	γ (10^{-3} cm^{-1})	d (cm)	$\langle \Delta H \rangle$ (10^{-5})	$\gamma d \langle \Delta H \rangle$ (10^{-6})
		Residual transverse polarization		
Vertical				
Scintillators	-3.9 ± 1.6	-0.37 ± 0.17	-4.7 ± 0.2	-0.07 ± 0.04
Ion chambers	-3.9 ± 2.2	-0.31 ± 0.17		-0.06 ± 0.05
Horizontal				
Scintillators	-6.2 ± 7.4	1.04 ± 0.41	$+3.5\pm0.5$	-0.23 ± 0.29
Ion chambers	-4.4 ± 8.4	0.34 ± 0.37		-0.05 ± 0.11
		Beam-matter interaction		
Position				
Scintillators	5.7 ± 0.3	0.11 ± 0.20		-2.19 ± 3.98
Ion chambers	6.0 ± 0.4	0.05 ± 0.02		-1.05 ± 0.43
			-350.0 ± 0.2	
Angle				
Scintillators	1.9 ± 0.3	$-0.8^{+0.15}_{-3.05}$		$0.55^{+1.0}_{-21.0}$

The terms for beam-matter interaction, which mostly affect I and U, are written

$$\sum \gamma_i d_i \langle \Delta H_i' \rangle = \gamma_3 (P_{1x} - P_{1x_0}) \langle \Delta R_{2y}' \rangle + \gamma_4 (P_{2x} - P_{1x} - P_0) \langle \Delta R_{2y}' \rangle , \quad (16)$$

where the last term contains the angle of the beam as determined from the P_1 and P_2 counters and P_0 is a constant for zero angle. It was found that this term was not needed for the ion-chamber system.

For each run, including calibration runs, the values of $\langle \Delta Z'/2Z' \rangle$, $\langle \Delta R_i' \rangle$, and $\langle P_i \Delta R_i' \rangle$ were found. The coefficients were determined with a χ^2 minimization procedure applied to these values. The 10% of the runs that contribute a $\chi^2 > 5$ to the fit were rejected. The results are given in Table IV. The $\chi^2/\mathrm{DF} = 1.17$ for both systems. The values of the coefficients and errors are those determined from the fit. Average values of $\langle \Delta H' \rangle$ are given, while the corrections were applied to each run. Thus the last column does not give the correlation actually applied. In particular, a strong correlation between position and angle in the beam-matter correction for scintillators gives misleading errors when the terms are taken separately.

V. RESULTS AND DISCUSSION

A. Result

Table V summarizes the values of $\langle \Delta Z'/2Z' \rangle'$ at each stage of the analysis and gives the result

$$\langle \Delta Z'/2Z' \rangle' = (-2.92\pm0.80)\times10^{-6} \quad (17)$$

for the scintillators and

$$\langle \Delta Z'/2Z' \rangle' = (-4.96\pm0.99)\times10^{-6} \quad (18)$$

for the ion chambers. Figure 6 shows a scatter plot of $\langle \Delta Z_1'/2Z_1' \rangle'$ vs $\langle \Delta Z_2'/2Z_2' \rangle'$. The correlation coefficient between values of $\langle \Delta Z'/2Z' \rangle'$ for the two detector systems is 0.20 and was determined from the values for each run after all the corrections were made. The small value of this coefficient indicates the measurements are essentially independent. A weighted average of Eqs. (17) and (18) gives

$$\langle \Delta Z'/2Z' \rangle' = (-3.73\pm0.62)\times10^{-6} . \quad (19)$$

The correction for the contribution from the correlation between transverse polarization and position in the beam is $\gamma\epsilon$, with ϵ given by Eq. (10). The value of γ is that given in Eq. (15), leading to a correction of $(-0.50\pm0.37)\times10^{-6}$ to $\langle \Delta Z'/2Z' \rangle'$. Thus the final value is

$$\langle \Delta Z'/2Z' \rangle' = (-3.23\pm0.72)\times10^{-6} . \quad (20)$$

The parity-nonconservation asymmetry A_L, defined in Eq. (1), is related to the net $\langle \Delta Z'/2Z' \rangle'$, in the limit of small ΔZ, by the expression

$$A_L = \frac{1}{|\vec{\mathbf{P}}| \ln Z} \left\langle \frac{\Delta Z'}{2Z'} \right\rangle' . \quad (21)$$

The result is

TABLE V. Summary of $\langle \Delta Z'/2Z' \rangle$ values for each stage of the analysis.

Stage of analysis	Scintillation counters	Ionization chambers
Raw asymmetry	$(-5.32\pm0.77)\times10^{-6}$	$(-6.66\pm0.87)\times10^{-6}$
After regression	-5.05 ± 0.69	-6.23 ± 0.84
Corrected for		
Transverse polarization	-4.75 ± 0.68	-6.14 ± 0.82
Beam-matter interaction	-2.92 ± 0.80	-4.96 ± 0.99

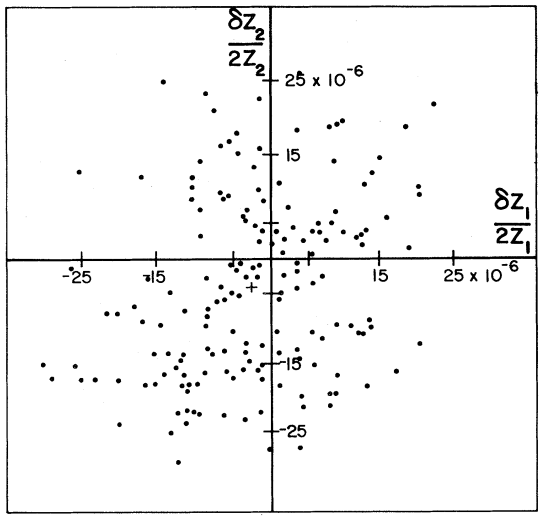

FIG. 6. Scatter plot of the transmission asymmetry from the two detector systems for each run. The averaged result is plotted with error bars and appears as a cross.

$$A_L = (2.65 \pm 0.60) \times 10^{-6} . \quad (22)$$

The error is statistical; it is dominated by the uncertainties in the individual measurements of the transmission that have been propagated through the analysis but also includes contributions from the statistical uncertainties in the corrections. The combined result gives a value for A_L more than four standard deviations from zero.

Several possible sources of false effects have been investigated and none proved significant. A change in beam momentum correlated with helicity would have caused problems. From the energy dependence of the cross section and an upper limit on the correlation between beam momentum and helicity, the effect is estimated to be $< 2 \times 10^{-7}$ and thus negligible. The effect of purely electronic sources of a false parity effect are tested by analyzing data taken with the beam off; the result is $A_L < 10^{-8}$. The result of analyzing the data grouped in a helicity-suppressing pattern is $A_L = (0.5 \pm 0.6) \times 10^{-6}$. A test of drifts in the signals is an analysis of alternate runs starting with the opposite polarization; the results with this analysis are unchanged.

Because the largest correction to $\langle \Delta Z'/2Z' \rangle$ comes from beam-matter interaction, several possible sources of error in the assumptions have been studied carefully. Data taken with the beam displaced 4 mm off the central axis yielded an unwanted 15% increase in the asymmetric halo measured at the I counter, due presumably to scattering from upstream apertures. However, the sensitivity of $\langle \Delta Z'/2Z' \rangle$ versus position agrees with a linear dependence within statistics. In addition, placement of the Lucite scatterer along the beam line was studied and the position chosen was representative of the real distribution of matter.[4] Finally, the introduction of additional scatterer upstream of the I counter did not change, within statistics, the asymmetric halo measured just downstream of the target. From these considerations we estimate a plausible systematic uncertainty of 20% of the correction, or 0.3×10^{-6}.

Another possible systematic error comes from uncertainties in the correction for the effect of polarization correlated with position within the beam. One contribution comes from our lack of direct knowledge of the shape of the polarization distribution across the beam profile. Another possible contribution is from the fact that the blocked-beam measurement was not taken at the location of the collimator. The total estimated uncertainty in the correction is 30%, leading to an estimated systematic uncertainty in the result of 0.2×10^{-6}. The measurement of this contribution was made near the end of the experiment; as a result we have no direct information on its stability with time. However, there is no evidence for drifts in the observed longitudinal asymmetry. If the observed asymmetry is the result of position-correlated polarization, this quantity must be large and constant during the long period of the data runs and then change abruptly to a small value at the point when it was measured. Such a change is very unlikely.

Other sources of systematic error, such as the treatment of residual transverse polarization and the effect of hyperon-decay products, are negligible. Combining the above uncertainties in quadrature the estimate for the overall systematic uncertainty in the result is 0.36×10^{-6}.

This leads to the final result

$$A_L = (2.65 \pm 0.60 \pm 0.36) \times 10^{-6} . \quad (23)$$

B. Comparison with theory

The asymmetry determined in this experiment is larger than expected from calculations of the interference between the weak and strong interactions at 6 GeV/c made prior to our experiment. Henley and Krejs[15] calculated A_L to be $\sim 1.0 \times 10^{-7}$ at 6 GeV/c. Modifications to the calculation by Desplanques, Donoghue, and Holstein[14] suggested the sign of A_L is positive at 6 GeV/c, but their calculation did not provide any substantial change in the magnitude of A_L. New meson-exchange calculations[17,18] have confirmed the results of the first one.[15] Other theoretical approaches include the multiperipheral model[19] and heavy boson exchange,[20] both of which also predict A_L to be at the level of $\sim 10^{-7}$.

The consistency between these calculations and their collective discrepancy with the experimental result have led theorists to consider other possibilities to account for the difference. The possibility of a contribution from Coulomb effects has been investigated[21] with the conclusion that only a 15% enhancement of the asymmetry is expected. Also, it has been noted[22] that strong enhancement of weak amplitudes could be important as in the case of nonleptonic strangeness-changing decays. A recent calculation used Regge theory to calculate the contribution to the asymmetry from parity nonconservation in the nucleon wave function.[23] The result is $A_L = +2.1 \times 10^{-6}$ with an estimated error of 30% but this calculation has been criticized[24] because its extension to low energies yields predictions for several parity-nonconservation results that are much larger than the experimental values.

Most recently a calculation has been reported that considers the effects of parity nonconservation at the quark level. This calculation included both the scattering contribution and the wave-function part.[25] The wave functions were written in the SU(6) quark basis. The calculation was done as an operator product expansion and independently by writing amplitudes for one-loop graphs. Single gluon exchange amplitudes were used for the strong interaction. The wave function mixing effect is based on a sum of transitions to negative parity excited nucleon states. The interaction takes place in the nucleon between one quark and a vector diquark. The results are dominated by the wave-function part with $A_L = +(0.7 \text{ to } 2.7) \times 10^{-6}$. Although this model is expected to be valid only at high energy and the uncertainty is large, the result is very encouraging.

This and most other calculations have been for proton-proton scattering and have not considered nuclear effects and the role of the neutrons. Although nuclear effects are not expected to be important at 6 GeV/c, they have not been excluded as a contributing factor. While this experiment was originally envisioned as a study of the weak interaction between nucleons, the most difficult parts of the problem for theorists are the strong interaction aspects. Much work remains to be done before a clear picture of the energy dependence of A_L emerges.

C. Discussion of previous runs at 6 GeV/c

Each version of this experiment has benefited from the earlier ones. The first measurement[1] at the ZGS found $A_L = (5.0 \pm 9.0) \times 10^{-6}$ using a Be target. This result is consistent with the present experiment. It was found that the dominant contribution to the fluctuations in the measurements of Z was due to nonuniformities in the target coupled with random motion of the beam. This lead us to use a water target with flat and parallel end windows in subsequent runs to ensure a uniform length and density for the target.

In the second version of this experiment,[2] A_L was found to be $(-15.0 \pm 2.4) \times 10^{-6}$. This value of A_L was attributed to the production of polarized hyperons in the target. A study[2] of the decay distribution of polarized Λ's with a Monte Carlo computer program, in which the longitudinal polarization transfer to the Λ's was assumed to be (0.26 ± 0.18), produced a cross-section asymmetry $A_L = (31 \pm 23) \times 10^{-6}$. The result of the present experiment using the T' detector, which reproduces the geometry of the detectors without the spectrometer, does not confirm the large negative asymmetry for the value of A_L but finds $A_L(T') = (3.9 \pm 0.72) \times 10^{-6}$ after all corrections.

The third experiment[3] included the spectrometer to eliminate hyperon-decay products. A large transverse scattering asymmetry due to the beam-matter interaction was discovered (six times greater than the present experiment). The result was $(-26.3 \pm 7.5) \times 10^{-6}$. Since the existence of the beam-matter interaction was not realized until the end of the third experiment, the data from the second experiment was not corrected for beam-matter interaction, nor was there an attempt to position the beam on the symmetry axis. Thus it is probable that beam-matter interaction was responsible for the large negative result in the second and third versions.

D. Considerations for future experiments

Additional information about the magnitude and energy dependence of A_L can be expected from future experiments. A transmission experiment[26] is underway at 1.5 GeV/c that expects an accuracy in the measurement of A_L of about 10^{-7}. Soon a polarization beam with a momentum range up to 28 GeV/c will be available for experiments at the Alternating Gradient Synchrotron at Brookhaven National Laboratory. In the next decade polarized beams at Fermilab may allow the search for parity-nonconserving front-back asymmetries in high-transverse-momentum proton-proton collisions. An angular distribution would yield more information than a total cross section measurement on the interference between the weak and strong scattering amplitudes of quarks and therefore aid in discriminating among strong interaction models.[27]

The experience gained from the ZGS experiments can provide guidelines for further experimental investigations. An attractive feature of the ZGS experiment was the ability to make two simultaneous independent measurements of A_L. Two detector systems with different properties increase the confidence in the final result by aiding in the understanding of systematic and random backgrounds. This experiment measured A_L with an accuracy of better than 6×10^{-7} in about a six-week period of data taking. The error is roughly 3 times greater than expected from the statistical fluctuations of the beam absorption in the target (Q factor ~ 3).

With the beam intensities above 5×10^8 protons/pulse, the Q factor increased rapidly, precluding a more precise measurement of A_L in a reasonable amount of time with these detectors. The extra fluctuations in the transmission measurement in each detector system are uncorrelated and therefore did not originate from a common source. It is now understood that the dominant source of noise for the ion chambers was due to spallation in the plates.[28] Beam motion during the spill, 60 Hz and greater, contributed to the noise for the scintillation counters. To improve the Q factor, a regression analysis removing beam motion from the transmission and a data selection procedure, during the spill, could be accomplished by electronically dividing the beam spill into small time segments. The gain drifts of both detector systems were random and negligible. Randomly selecting the sign of the initial polarization might reduce the effects of long-term drifts.

The next measurement of A_L at high energy should have an accuracy at the 10^{-7} level. This would require at least 10^{15} protons on target and therefore a more intense beam. Ion chambers perform well in intense beams but scintillation counters do not because of radiation damage to the plastic scintillator. The use of liquid scintillator instead of plastic scintillator is a possible solution to this problem. Alternatively, an experiment that measures only the scattered beam from the target with scintillation counters and the transmitted beam with ion chambers

could utilize high beam intensities.

The credibility of such experiments depends on the identification and study of all sources of systematic error greater than approximately half of the desired statistical accuracy. This is no easy task as there is no global test to determine the presence of a systematic contribution to A_L. An experiment measuring A_L at the 10^{-7} level will consider systematic effects that were negligible in this experiment. Therefore, careful consideration should be given to detector systems that monitor beam properties and the models used to make corrections should be experimentally tested. Also, classes of systematics may be studied with unpolarized beam.

In the present experiment the contribution from beam-matter interaction was reduced by evacuating the beam line where possible, adding helium elsewhere, and enlarging the aperture at the entrance to the experimental area just upstream of $B2$. Even so, the largest systematic correction to A_L in the present experiment comes from the beam-matter interaction. The correction to A_L, with the beam carefully positioned on the symmetry axis, is $\sim 1.2\times 10^{-6}$. Transporting a longitudinally polarized beam to the experimental area would eliminate this contribution to A_L. Otherwise beam halo can be a very subtle and time-dependent source of systematic error.

The method used in this experiment to measure residual-transverse-polarization contributions to A_L could be repeated in a more sensitive measurement of A_L. A position-feedback loop controlling the current in an upstream bending magnet is necessary to minimize beam motion and maintain the beam position on the symmetry axis to minimize effects of residual transverse polarization. Control runs in general should be repeated frequently during the experiment to compensate for changing conditions.

The correlation of polarization with phase space should be measured at apertures that intercept scattered beam and can be determined by passing a thin scatterer through the beam and measuring the resulting transverse scattering asymmetry.[29]

E. Conclusions

We have measured the parity-nonconserving helicity dependence of the total cross section for 6-GeV/c polarized protons on a water target. The result is $A_L=(2.65\pm 0.60\pm 0.36)\times 10^{-6}$. The first error is statistical and the second is an estimate of the contribution from systematic uncertainties. This indicates a strong energy dependence associated with the weak or hadronic interaction between nucleons as the lower-energy measurements yield $A_L\sim 10^{-7}$. Such a large energy dependence was not expected although it may be understood through recent calculations at the quark level.

ACKNOWLEDGMENTS

We thank the staff of the Argonne National Laboratory ZGS complex for their support and hospitality. In addition, we are grateful to S. Johnson, T. Lopez, J. Sandoval, L. Sorensen, B. Nelson, W. Purcell, G. Pares, J. Gehrke, and P. Eder for help during the experiment, and to R. Winston for his general assistance and for the use of the NOVA-820 computer. We thank H. L. Anderson and R. Gabriel for their support and for use of their ionization chambers. We also thank E. Henley, H. Frauenfelder, and C. Barnes for their continued interest and encouragement of R. G. H. Robertson for a critical reading of the manuscript. This work was supported in part by the U.S. Department of Energy and the National Science Foundation.

*Present address: Stanford Linear Accelerator Center, P.O. Box 4349, Stanford, CA 94305.

†Present address: University of Maryland, College Park, MA 20742.

‡Permanent address: Elmhurst College, Elmhurst, IL 60106.

§Present address: Los Alamos National Laboratory, Los Alamos, NM 87545.

**Present address: Bell Laboratories, Naperville, IL 60566.

††Present address: Bell Laboratories, P.O. Box 400, Holmdel, NJ 07733.

[1]J. D. Bowman, C. M. Hoffman, C. F. Hwang, R. E. Mischke, D. E. Nagle, J. M. Potter, D. M. Alde, P. G. Debrunner, H. Frauenfelder, L. B. Sorensen, H. K. Anderson, and R. Talaga, Phys. Rev. Lett. **34**, 1184 (1975).

[2]R. L. Talaga, Ph.D. dissertation, University of Chicago, 1976.

[3]D. M. Alde, Ph.D. dissertation, University of Illinois, 1978.

[4]N. S. Lockyer, Ph.D. dissertation, Ohio State University, 1980.

[5]N. Lockyer, T. A. Romanowski, J. D. Bowman, C. M. Hoffman, R. E. Mischke, D. E. Nagle, J. M. Potter, R. L. Talaga, E. C. Swallow, D. M. Alde, D. R. Moffett, and J. Zyskind, Phys. Rev. Lett. **45**, 1821 (1980).

[6]D. E. Nagle *et al.*, in *High Energy Physics with Polarized Beams and Targets,* proceedings of the Third International Symposium, Argonne, 1978, edited by G. H. Thomas (AIP, New York, 1978), p. 224.

[7]R. Balzer, R. Henneck, Ch. Jacquemart, J. Lang, M. Simonius, W. Haeberli, Ch. Weddigen, W. Reichart, and S. Jaccard, Phys. Rev. Lett. **44**, 699 (1980).

[8]M. Simonius, in *High-Energy Physics with Polarized Beams and Polarized Targets,* proceedings of International Symposium, Lausanne, Switzerland, 1980, edited by C. Joseph and J. Soffer, Experientia Supplementum Vol. 38 (Birkhäuser, Basel, Switzerland, 1981), p. 355.

[9]V. R. Brown, E. M. Henley, F. R. Krejs, Phys. Rev. Lett. **30**, 770 (1973); Phys. Rev. C **9**, 935 (1974).

[10]M. Simonius, Phys. Lett. **41B**, 415 (1972); Nucl. Phys. **A220**, 269 (1974).

[11]Y. Yamamoto, Prog. Theor. Phys. **58**, 1790 (1977).

[12]G. N. Epstein, Phys. Lett. **55B**, 249 (1975).

[13]B. H. J. McKellar and K. R. Lassey, Phys. Rev. C **17**, 842 (1978).

[14]B. Desplanques, J. F. Donoghue, and B. R. Holstein, Ann. Phys. (N.Y.) **124**, 449 (1980).

[15]E. M. Henley and F. R. Krejs, Phys. Rev. D **1**, 605 (1975).

[16]V. B. Kopeliovich and L. L. Frankfurt, Pis'ma Zh. Eksp. Teor. Fiz. **22**, 601 (1975) [JETP Lett. **22**, 295 (1975)].

[17]T. Oka, Prog. Theor. Phys. **66**, 977 (1981).
[18]A. Barroso and D. Tadić, Nucl. Phys. **A364**, 194 (1981).
[19]L. L. Frankfurt and M. I. Strikman, Phys. Lett. **107B**, 99 (1981).
[20]J. Soffer, in *High-Energy Physics with Polarized Beams and Polarized Targets* (Ref. 8), p. 370; P. Chiappetta, J. Soffer, and T. T. Wu, J. Phys. G **8**, L93 (1982).
[21]A. S. Goldhaber, Phys. Rev. D **25**, 715 (1982).
[22]A. S. Goldhaber, T. Goldman, and D. Preston, Phys. Rev. Lett. **48**, 214 (1982).
[23]G. Nardulli and G. Preparata, Phys. Lett. **117B**, 445 (1982).
[24]J. F. Donoghue and B. R. Holstein, Phys. Lett. **125B**, 509 (1983).
[25]T. Goldman and D. Preston, Nucl. Phys. **B217**, 61 (1983).
[26]D. E. Nagle, J. D. Bowman, R. Carlini, R. E. Mischke, H. Frauenfelder, R. W. Harper, V. Yuan, A. B. McDonald, and R. Talaga, in *High Energy Spin Physics—1982,* proceedings of the 5th Symposium, Brookhaven National Laboratory and Westhampton Beach, New York, edited by G. M. Bunce (AIP, New York, 1983), p. 150.
[27]E. Fischbach and G. W. Look, Phys. Rev. D **16**, 2199 (1977).
[28]J. D. Bowman, R. Carlini, R. Damjanovich, R. E. Mischke, D. E. Nagle, R. L. Talaga, R. W. Harper, and V. Yuan, Nucl. Instrum. Methods **216**, 399 (1983).
[29]W. Haeberli, R. Hennick, Ch. Jacquemart, J. Lang, R. Müller, M. Simonius, W. Reichart, and Ch. Weddigen, Nucl. Instrum. Methods **163**, 403 (1979).